Materials Transactions, Vol. 67, No. 4 (2026) pp. 425 to 431

High Aspect Ratio of Silver Nanowires for Ultralow Chemical Concentration Detection via Surface-Enhanced Infrared Absorption Spectroscopy

Thi Kim Hang Pham[1], Thi Thu Linh Tran[1], Bao Quan Tran[1], Thi Hang Nguyen[1], Thi Minh Nguyet Nguyen[2], Thi Hue Do[2], Thi Thanh Hoa Pham[3] and Hai Dang Ngo[1,*]

[1]*Faculty of Applied Sciences, Ho Chi Minh University of Technology and Engineering, Ho Chi Minh City 72000, Vietnam*
[2]*Faculty of Physics, Thai Nguyen University of Education, Thai Nguyen City 24000, Vietnam*
[3]*Faculty of Engineering and Technology, Van Hien University, Ho Chi Minh City 72000, Vietnam*

Plasmonic nanomaterials (Au, Ag, Pt, and Cu) have attracted attention for enhanced spectroscopic sensing applications. Different approaches have been developed for nanostructure synthesis. In this study, high aspect ratio silver nanowires were successfully synthesized using the polyol method. During the preparation step, iron (III) chloride was introduced as a catalytic agent to help the nanowires development. The influence of $FeCl_3$ reduction time on the morphology and plasmonic behavior of silver nanowires was systematically investigated. The UV-Vis spectra of silver nanowires presented a main absorption peak around 400 nm and a prominent shoulder around 350 nm. Scanning electron microscopy images confirmed the micrometer-scale lengths and narrow diameters. Furthermore, low-cost Surface-Enhanced Infrared Absorption Spectroscopic substrates were fabricated by depositing silver nanowires onto filter paper. Owing to the strong localized surface plasmon resonance of metallic nanostructures, the silver nanowires-based substrates enabled ultrasensitive detection of Eosin Y down to 10 ppb. The study highlighted the key role of iron (III) chloride in silver nanowire synthesis and demonstrated the facile economical preparation of silver nanowire-on filter-paper substrates as chemical sensors for trace-level detection. [doi:10.2320/matertrans.MT-M2025154]

(Received November 25, 2025; Accepted January 14, 2026; Published March 25, 2026)

Keywords: *silver nanowire, catalyst, surface-enhanced infrared absorption, chemical sensors, field enhancement*

1. Introduction

Noble metal nanostructures have gained considerable attention thanks to not only significant advances in synthesis, manipulation but also their unique chemical and physical properties as well [1–3]. Among this large family, silver nanowires (AgNWs) are considered critical nanomaterials in various fields such as biomedicine, sensing, optics, and electrical circuits due to their interesting properties, such as outstanding electrical conductivity, strong antibacterial effects, and remarkable optical characteristics [4–9]. However, the controlled synthesis and morphology regulation of AgNWs remains a key challenge, which limits their full exploitation in practical applications [10–12].

Different methods, including chemical reduction, evaporation-condensation, laser ablation, and biological processes, have been utilized to tailor silver nanostructures [13]. For silver nanowire synthesis, chemical reduction is one of the most popular technique, whereby silver ions (Ag^+) can be easily reduced to neutral atoms (Ag) by various agents. The presence of a stabilizing agent such as polyvinyl-pyrrolidone (PVP) plays a crucial role in the development of the nanowires and prevents the undesired aggregation of Ag particles [14]. During the process, Ag atoms nucleate into seeds and subsequently grow into nanowires particles, reaching a supersaturated level. This method maximizes the material's specific characteristics by ensuring the consistency of AgNWs and enabling precise control over the production process.

Iron (III) chloride ($FeCl_3$), a well-known catalyst, can accelerate the reduction rate in the synthesis of silver nanowires due to the presence of Fe^{3+} [15, 16]. The duration of $FeCl_3$-mediated reduction is expected to significantly influence the dimensions, morphology, and characteristics of the resulting AgNWs. Nonetheless, systematic investigations focusing on the effect of $FeCl_3$ reduction duration on the AgNW growth and plasmonic behavior remain limited. Understanding the relationship is essential for the optimization of the synthesis process and enabling the modification of material properties to satisfy particular requirements for the application.

In the detection of ultralow chemical concentrations, two methods have been proposed and continuously improved: Surface-enhanced Raman spectroscopy (SERs) and Surface-Enhanced Infrared Absorption Spectroscopy (SEIRA). Each presents different pros and cons. They both rely on the plasmon resonance effect of noble metallic nanostructures to amplify the Raman or infrared signals of the sensed chemicals. Thanks to the field enhancement effect, those signals can be vastly intensified even trace-level concentration of parts per million (ppm) or parts per billion (ppb).

In this work, AgNWs were synthesized via a chemical reduction route with $FeCl_3$ as a catalytic agent. The influence of reduction duration on their structure, size, and optical properties of the AgNWs was systematically examined. The findings could provide a better understanding of the AgNW growth mechanism. Furthermore, the as-synthesized AgNWs were anchored onto filter paper to fabricate low-cost SEIRA substrates. Employing the localized surface plasmon resonance in AgNWs, the fabricated substrates significantly enhanced the infrared absorption signals of Eosin Y (EY) indicator molecules at ultralow chemical concentrations [17–19]. In this work, EY residues are detectable down to 10 ppb, owing to the strong localized electromagnetic fields generated around AgNWs, which enhance molecular vibrational modes and significantly amplify the infrared absorption signals through the field enhancement effect. Randomly anchored AgNWs respond to non-polarized incident infrared

*Corresponding author, E-mail: dangnh@hcmute.edu.vn

light and generate a great number of plasmonic hotspots, especially at acute tips and narrow junctions between the wires. Consequently, SEIRA based on AgNWs demonstrates enhanced efficiency and exceptional sensitivity where the enhancement factor can be approximately two orders of magnitude. These findings provide insights into controlled AgNW synthesis and demonstrate a simple, low-cost route toward efficient SEIRA substrates for trace-level chemical detection.

2. Experimental Procedure

The synthesis of silver nanowires via the polyol method is schematically described in Fig. 1. The process begins with the preparation of a mixture consisting of 8.75×10^{-7} mol PVP in 20 mL ethylene glycol (EG). The solution was placed in a round-bottom flask, continuously stirred, and maintained at a temperature of 160°C using a magnetic stirrer. After the temperature stabilizes for about 10 minutes, an amount of $FeCl_3$ was added to initiate the reduction stage. The solution continues to be stirred at different reduction intervals (T = 15, 20, and 30 minutes) to investigate the influence of this duration on the formation of nanowires. Next, 6.48×10^{-4} mol of $AgNO_3$ was added to the flask and stirred continuously until the solution turned a cloudy silver color, indicating the formation of silver nanowires. Finally, the silver colloidal solution was rapidly cooled by immersing the flask in ice water.

Subsequently, filter paper with dimensions of $1.5 \times 1.5\ cm^2$ was fully sonicated in the Ag nanowire colloidal solution for 5 minutes and then kept immersed for an additional 5 minutes to allow anchoring of AgNWs. The filter paper was allowed to dry in ambient air for 30 minutes. The soaking and drying procedure was performed three consecutive times to enhance the density and adherence of AgNWs on the filter paper. The paper fragments were dipped in Eosin Y ($C_{20}H_6Br_4Na_2O_5$) solution at varying concentrations for 30 seconds, subsequently dried at room temperature, and then analyzed by FT-IR spectroscopy (Perkin Elmer).

3. Results and Discussions

The effect of $FeCl_3$ reduction time on the morphology and size evolution of silver nanostructures was analyzed through scanning electron microscopic (SEM, Hitachi 4800) imaging. As shown in Fig. 2(a) and 2(b), both $FeCl_3$-15 min and $FeCl_3$-20 min samples, exhibit the coexistence of spherical nanoparticles and short nanowires, with a large number of particles interspersed among the rods and wires. This morphology suggests that the system remains in a mixed or transitional growth regime. Ag nanowires in the $FeCl_3$-15 min sample display diameters ranging from 54 to 107 nm and lengths ranging from 2386 to 6188 nm, while the spherical particles have diameters ranging from 57 to 142 nm (Fig. 2(a)). Similarly, the $FeCl_3$-20 min sample presents the nanowires with diameters of 37–114 nm and lengths ranging from 1099 to 4135 nm, while the spherical particles have diameter ranging from 45–97 nm. These observations are consistent with the statistical size distributions summarized in Table 1.

In contrast, the $FeCl_3$-30 min sample (Fig. 2(c)) presents a well-defined nanowire-dominated morphology, characterized by lengths (2477–6355 nm) and relatively narrow diameters (44–180 nm). As the reduction time of $FeCl_3$ increases, the presence of Cl^- ions in the solution is prolonged, facilitating the formation of AgCl, which acts as seeds for the formation of pentagonal nuclei [20]. These nuclei, along with the high concentrations of Cl^- and O_2, can induce severe corrosion on the surface of silver nanowires, resulting in the formation of a large number of spherical silver nanoparticles [21, 22]. This process reduces the efficiency of forming the desired nanowires. However, when the reduction time is further extended, Fe^{3+} ions in the solution are gradually reduced to Fe^{2+} in the ethylene glycol (EG) environment. The presence of Fe^{2+} at an adequate level helps to reduce O_2 - a factor contributing to corrosion [20]. As a result, this process leads to selective corrosion, leaving behind pentagonal nuclei, which are crucial factors in the formation and growth of additional silver nanowires. As a result, AgNWs synthesized at 30 min exhibit much higher aspect ratios than those

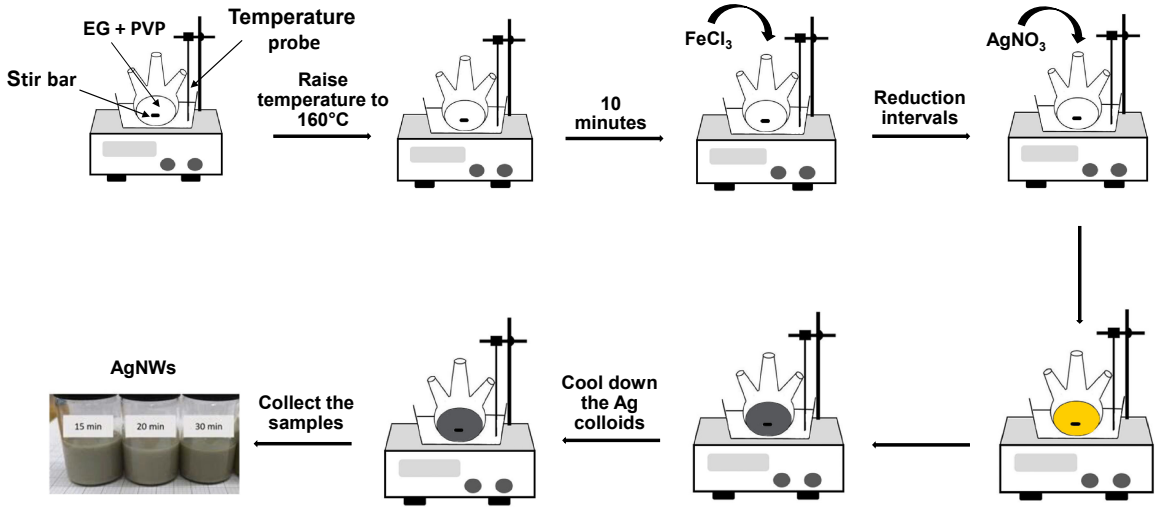

Fig. 1 Schematic illustration of the AgNWs synthesis process. (online color)

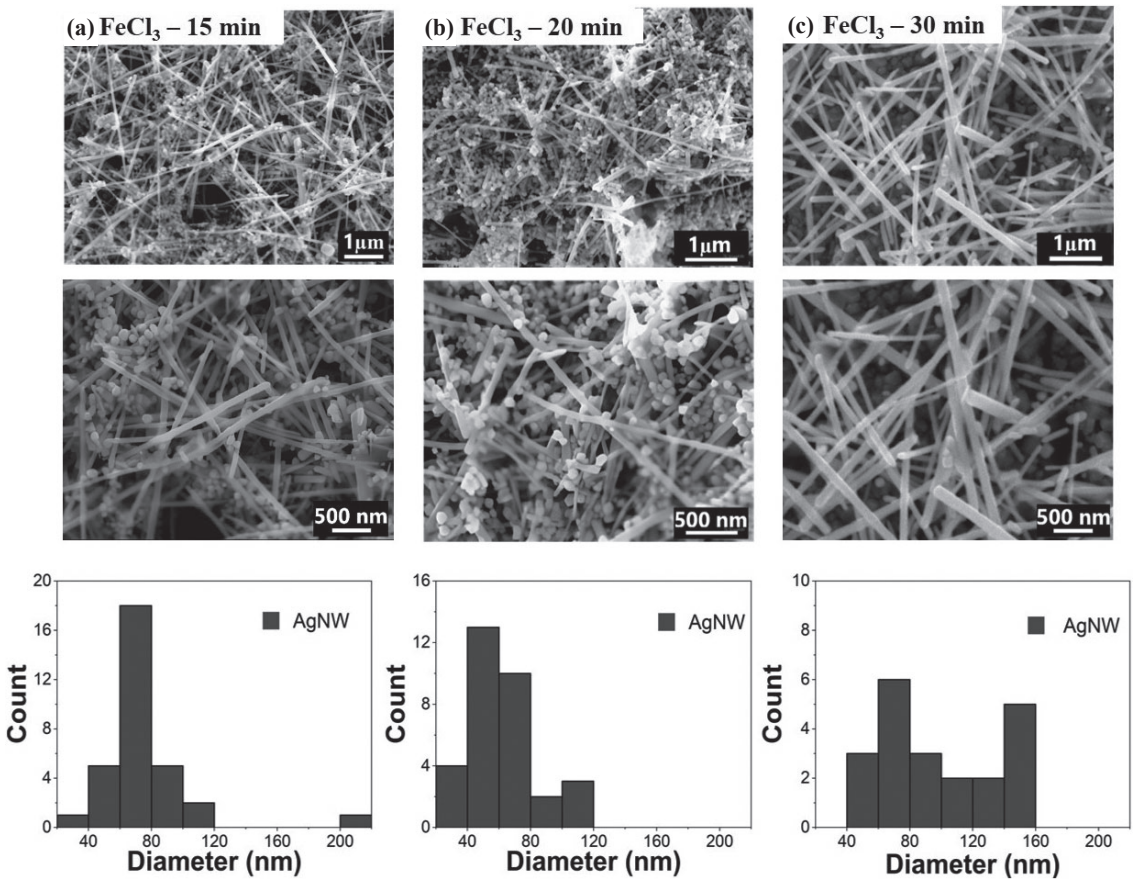

Fig. 2 SEM images and diameter distribution of AgNW samples (a) $FeCl_3$–15 min, (b) $FeCl_3$–20 min, and (c) $FeCl_3$–30 min.

Table 1 Size of nanostructure silver in the sample $FeCl_3$-15 min, $FeCl_3$-20 min, and $FeCl_3$-30 min.

Sample	Ag nanowire			Ag nanoparticles
	Length (nm)	Diameter (nm)	Aspect ratio	Diameter (nm)
$FeCl_3$-15 min	2386 - 6118	54 – 107	44 - 57	57 – 142
$FeCl_3$-20 min	1099 - 4135	37 – 114	30 - 36	45 – 97
$FeCl_3$-30 min	2477 – 6355	44 – 180	56 - 35	-

obtained at shorter reduction times. Such high ratios are necessary for shifting the plasmon resonance of PVP-coated Ag NWs to infrared region, which is essential for effective SEIRA applications.

The influence of the reduction time of $FeCl_3$ on the formation of Ag nanoparticles and nanowires is clearly illustrated by UV-Vis absorption spectra (Jasco V-730) (Fig. 3). Obviously, there are two peaks corresponding to the primary and secondary surface plasmon resonances (a broad peak and a shoulder) are located in the range of 350–450 nm. The position and intensity of the resonance peaks depend on the size and aspect ratio of the silver nanowires [23]. Two peaks of the $FeCl_3$-15 min, $FeCl_3$-20 min and the $FeCl_3$-30 min samples are located at 351 nm and 405 nm; at 352 nm and 407 nm; at 352 nm and 387 nm, respectively. As the reduction time of $FeCl_3$ increases, especially the $FeCl_3$-30 min sample, the primary broad peak shifts toward the

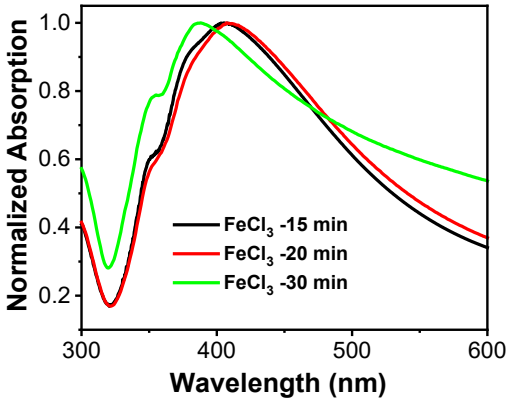

Fig. 3 Normalized UV-Vis absorption spectra of the AgNW samples. (online color)

Table 2 Optical property parameters of the Ag nanostructure.

Sample	Secondary Peak AgNW (I)	Primary Peak AgNP (I_o)	Ratio I/I_o
$FeCl_3$-15 min	0.608 (λ = 351nm)	1 (λ = 405nm)	0.61
$FeCl_3$-20 min	0.579 (λ = 352nm)	1 (λ = 407nm)	0.58
$FeCl_3$-30 min	0.781 (λ = 352nm)	1 (λ = 387nm)	0.78

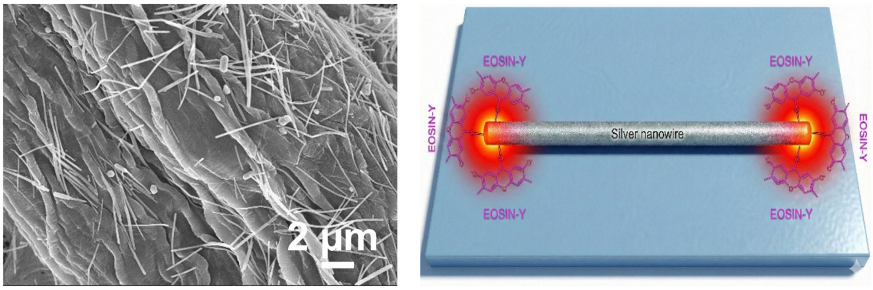

Fig. 4 SEM images of AgNWs anchored on filter paper (left) and field enhancement at two ends of AgNWs (right). (online color)

shorter wavelength. However, the peak shift does not follow a monotonic trend. The $FeCl_3$–20 min sample exhibits negligible or slightly red-shifted behavior, suggesting a critical reduction time for effective plasmonic evolution.

This can be explained by the prolonged reduction time, which allows more Ag^+ ions to be reduced to Ag^0, and consequently, the size of the silver nanoparticles increases [23]. In addition, the presence of small particles on the surface of the rods and wires contributes to the shift in the absorption peak [24]. During the synthesis process, the shape and size of the nanoparticles also change. The initial nanoparticles develop to form nanorods, which then gradually extend into nanowires. Over time, these nanoparticles transform into AgNWs and continue to grow, with two characteristic resonance peaks appearing at 350 nm and 377 nm ($FeCl_3$-30 min sample), as reported in previous studies [25].

Ag nanoparticle (AgNP) content in the samples also decreases over different $FeCl_3$ reduction time. As the reduction time of $FeCl_3$ gradually increases, the I/I_o ratio reaches values of 0.61, 0.58, and 0.78, respectively. The higher I/I_o value obtained for the $FeCl_3$-30 min sample indicates that AgNW formation predominates over the AgNP formation. The results confirm a clear transition from nanoparticle-rich to nanowire-dominated structures with prolonged reduction time. The optical characteristics of the Ag nanostructure are outlined in Table 2.

Successful anchoring of AgNWs onto filter paper is clearly illustrated in Fig. 4 (left). Evidently, a huge quantity of AgNWs adheres randomly to the paper surface and within different holes. This facilitates effective contact of AgNWs to EY molecules at plasmonic hotspots, especially at acute tips and narrow junctions between the wires (Fig. 4, right). It also mediates good response of SEIRA substrates to an unpolarized infrared beam.

Figure 5 displays the FT-IR spectra of Eosin Y dye at different concentrations (ppm and ppb levels) on filter paper and SEIRA substrates in the fingerprint region of 2500–4000 cm^{-1}. Infrared signals of Eosin Y exhibit an absorption band at wavenumbers 2850–2950 cm^{-1}, corresponding to the stretching vibrations of the methyne C-H group and the C=C bond within the aromatic ring of the Eosin Y structure [26]. The pronounced absorption peak in the wavenumber range of 3200 to 3400 cm^{-1} relates to the stretching vibration of the O-H hydrogen bond [26]. The peak position varies marginally from 3232 to 3239 cm^{-1} based on the EY concentration, indicating alterations in the hydrogen bonding environment at different concentration levels. The presence of AgNWs on SEIRA substrates results in a substantial enhancement of the infrared signals within the 1–10 ppm (Fig. 5(a)) and 10–500 ppb (Fig. 5(b)) regions. This demonstrates that the infrared signal of the Eosin Y solution is markedly amplified on the SIERA substrate, attributable to the surface plasmon resonance phenomenon.

The enhancement factor (EF) is calculated using the formula:

$$EF = (I_{\text{Seira}}/I_{\text{FT-IR}}) * (n_{\text{FT-IR}}/n_{\text{Seira}})$$

where I_{Seira} and n_{Seira} are the intensity of the FT-IR peak and concentration of the Eosin-Y molecule absorbed on the SEIRA substrate, respectively. Similarly, $I_{\text{FT-IR}}$ and $n_{\text{FT-IR}}$ are the intensity of the FT-IR peak and concentration of Eosin-Y absorbed on trivial filter paper. The data in Table 3 indicate that at low concentrations (ppm level), the enhancement factor is roughly 97–98, diminishing slightly to approximately 92–93 times when the concentration of EY reaches

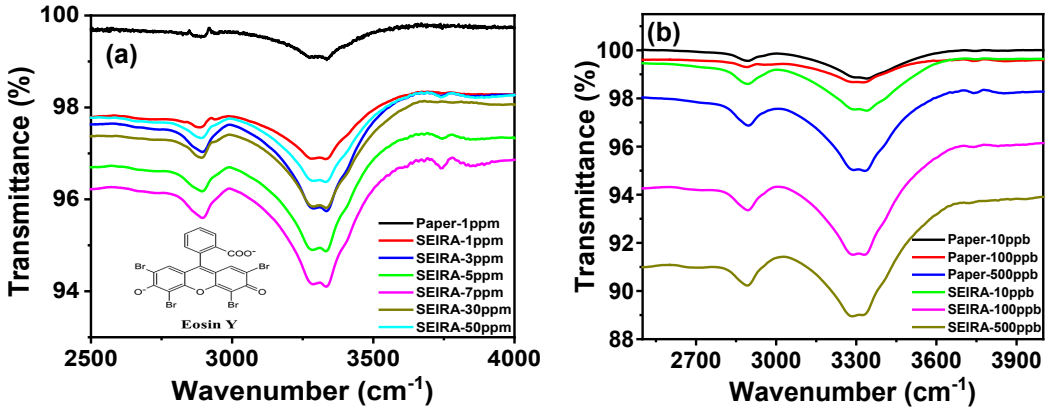

Fig. 5 FTIR signals of the Eosin-Y on filter paper and SEIRA substrates at ppm (a) and ppb (b) levels. (online color)

Table 3 Effectiveness of SEIRA substrate in enhancing EY detection at low concentrations.

Concentration EY	Reference Peak (I_1)	SEIRA Peak (I_2)	Ratio I/I_1
10ppb	98.83	97.49	0.99
100ppb	98.68	91.51	0.93
500ppb	94.99	88.95	0.94
1ppm	99.07	96.85	0.98
3ppm	98.42	95.69	0.97
5ppm	97.53	94.82	0.97
7ppm	96.14	94.03	0.98
30ppm	97.78	95.78	0.98
50ppm	97.97	96.35	0.98

about 100 ppb and 500 ppb. Even at an ultralow concentration of 10 ppb, the SEIRA enhanced signals were clear and sufficient for quantitatively assessment. Furthermore, the enhancement factor increased by 98 times, markedly surpassing the values observed at concentrations of 100 ppb and 500 ppb. The cause is attributed to the uneven distribution of EY on the AgNWs surface, the contact among EY dye molecules, or the chemical interaction between EY and the PVP coating, which diminishes absorption and impacts SEIRA signal amplification [27]. Concurrently, the diminished quantity of EY molecules elevates the likelihood of these molecules residing in hotspot locations—localized nanoscale regions where the electric field is markedly intensified due to the surface plasmon resonance effect, resulting in amplified signals at exceedingly low concentrations [28]. The analytical results indicate that the SEIRA substrate is proficient in detecting EY at low concentrations between 50 ppm and 10 ppb. Consequently, AgNWs possess prospective uses in environmental sectors, organic residue analysis, and highly sensitive chemical sensors.

The high aspect ratio of the AgNWs, particularly in the $FeCl_3$-30 min sample, plays a crucial roles in achieving the 10 ppb detection limit. Firstly, the longitudinal plasmonic modes of high-aspect-ratio nanowires are known to extend into the infrared region, providing the necessary spectral overlap for SEIRA enhancement. This shift is essential because effective SEIRA requires spectral overlap between the metallic nanostructure's resonance and the vibrational modes of the target molecule. For Eosin Y, these modes appear in the 2500–4000 cm^{-1} range. The high aspect ratio ensures that the AgNWs act as efficient nanoantennas for these infrared frequencies. Secondly, randomly anchored AgNWs on filter paper respond to non-polarized incident infrared light and generate a significant number of plasmonic hotspots. These hotspots are localized primarily at the acute tips and at narrow junctions where wires overlap. As the aspect ratio increases, the probability of forming these narrow junctions on the filter paper increases, providing more active sites for Eosin Y molecules to experience field enhancement. These hotspots significantly amplify the molecular vibra-

tional modes of Eosin Y, leading to the observed enhancement factor of approximately 98 at ultralow concentrations. Finally, the high aspect ratio ensures a large surface-area-to-volume ratio, facilitating a high density of Eosin Y molecules in contact with plasmonic hotspots. This geometric advantage allows us to achieve an enhancement factor of approximately 98 times, even at an ultralow concentration of 10 ppb. Without these high aspect ratio structures, the field enhancement would be insufficient to detect trace-level organic residues at the parts-per-billion level.

However, despite the high aspect ratio of silver nanowires, the enhancement factor is still lower than expected, since the plasmon resonance frequency of PVP-coated AgNWs probably locates somewhere in the near-infrared region. To further increase the enhancement factor, the plasmon resonance frequency should be shifted to infrared region; therefore, AgNWs should be coated with other high-dielectric-constant materials such as ZnO or TiO_2.

4. Conclusion

In this report, silver nanowires (AgNWs) were successfully synthesized using the polyol method, with $FeCl_3$ serving as a critical reaction catalyst. Increasing the FeCl3 reduction time from 15 to 30 min effectively promoted AgNW formation, leading to an optimized nanowire-dominated morphology characterized by high aspect ratios, nanoscale diameters, and micrometer-scale lengths reaching up to 6355 nm. This study highlights that achieving the high-aspect-ratio is fundamental for shifting the plasmon resonance into the infrared region, which is essential for effective SEIRA applications. The as-prepared AgNWs were anchored onto filter paper to fabricate low-cost SEIRA substrates. These substrates exhibited strong performance for Eosin Y detection over a wide concentration range from 50 ppm down to 10 ppb. The fingerprint infrared peaks of Eosin Y were significantly amplified due to the strong localized electromagnetic fields generated by the high-aspect-ratio nanowires, particularly at acute tips and narrow junctions. Enhancement factors reached approximately 98 times at the 10 ppb level. These results demonstrate that the $FeCl_3$-assisted synthesis of high-aspect-ratio AgNWs provides a facile, economical route for creating sensitive chemical sensors. The high aspect ratio not only optimizes the spectral response but also maximizes the density of plasmonic hotspots, making these substrates highly effective for the quantitative detection of organic pollutants and toxic chemicals at extremely low concentrations.

Acknowledgments

This work belongs to the project T2025-129 funded by Ho Chi Minh City University of Technology and Engineering, Ho Chi Minh City, Vietnam.

REFERENCES

[1] M.T. Aminzai, M. Yildirim and E. Yabalak: Metallic nanoparticles unveiled: Synthesis, characterization, and their environmental, medicinal, and agricultural applications, Talanta **280** (2024) 126790.

[2] M. Shahalaei, A.K. Azad, W.M.A.W. Sulaiman, A. Derakhshani, E.B. Mofakham, M. Mallandrich, V. Kumarasamy and V. Subramaniyan: A review of metallic nanoparticles: present issues and prospects focused on the preparation methods, characterization techniques, and their theranostic applications, Front Chem. **12** (2024) 1398979.

[3] K. Toisawa, Y. Hayashi and H. Takizawa: Synthesis of highly concentrated Ag nanoparticles in a heterogeneous solid-liquid system under ultrasonic irradiation, Mater. Trans. **51** (2010) 1764–1768.

[4] M.-G. Kang, T. Xu, H.J. Park, X. Luo and L.J. Guo: Efficiency enhancement of organic solar cells using transparent plasmonic Ag nanowire electrodes, Adv. Mater. **22** (2010) 4378–4383.

[5] M. Song, G. Chen, Y. Liu, E. Wu, B. Wu and H. Zeng: Polarization properties of surface plasmon enhanced photoluminescence from a single Ag nanowire, Opt. Express **20** (2012) 22290–22297.

[6] L. Gou, M. Chipara and J.M. Zaleski: Convenient, rapid synthesis of Ag nanowires, Chem. Mater. **19** (2007) 1755–1760.

[7] E. Matras, A. Gorczyca, E. Pociecha, S.W. Przemieniecki and M. Oćwieja: Phytotoxicity of silver nanoparticles with different surface properties on monocots and dicots model plants, J. Soil Sci. Plant Nutr. **22** (2022) 1647–1664.

[8] A. Jouyban and E. Rahimpour: Optical sensors based on silver nanoparticles for determination of pharmaceuticals: An overview of advances in the last decade, Talanta **217** (2020) 121071.

[9] B. Calderón-Jiménez, M.E. Johnson, A.R. Montoro Bustos, K.E. Murphy, M.R. Winchester and J.R. Vega Baudrit: Silver nanoparticles: Technological advances, societal impacts, and metrological challenges, Front Chem. **5** (2017) 6.

[10] M. Lagrange, D.P. Langley, G. Giusti, C. Jiménez, Y. Bréchet and D. Bellet: Optimization of silver nanowire-based transparent electrodes: effects of density, size and thermal annealing, Nanoscale **7** (2015) 17410–17423.

[11] S.M. Bergin, Y.-H. Chen, A.R. Rathmell, P. Charbonneau, Z.-Y. Li and B.J. Wiley: The effect of nanowire length and diameter on the properties of transparent, conducting nanowire films, Nanoscale **4** (2012) 1996–2004.

[12] D.H.T. Linh, N.P. Anh, T.T.A. Mi, N.T. Tinh, H.T. Cuong, T.L. Quynh, N.T.T. Van, N.V. Minh and N. Tri: Biosynthesis, characteristics and antibacterial activity of silver nanoparticles using lemon citrus latifolia extract, Mater. Trans. **59** (2018) 1501–1505.

[13] S. Iravani, H. Korbekandi, S.V. Mirmohammadi and B. Zolfaghari: Synthesis of silver nanoparticles: chemical, physical and biological methods, Res. Pharm. Sci. **9** (2014) 385–406.

[14] W. Huang, L. Zhang, Q. Yang and Z. Wang: Polyvinylpyrrolidone as an efficient stabilizer for silver nanoparticles, Chin. J. Chem. **32** (2014) 909–913.

[15] N.M. Abbasi, H. Yu, L. Wang, Zain-ul-abdin, W.A. Amer, M. Akram, H. Khalid, Y. Chen, M. Saleem, R. Sun and J. Shan: Preparation of silver nanowires and their application in conducting polymer nanocomposites, Mater. Chem. Phys. **166** (2015) 1–15.

[16] X.-M. Wang, L. Chen, E. Sowade, R.D. Rodriguez, E. Sheremet, C.-M. Yu, R.R. Baumann and J.-J. Chen: Ultra-uniform and very thin ag nanowires synthesized via the synergy of cl–, br– and Fe3+ for transparent conductive films, Nanomaterials **10** (2020) 237.

[17] M. Osawa: Surface-enhanced infrared absorption, *Near-field Optics and Surface Plasmon Polaritons*, (Springer, 2006) pp. 163–187.

[18] J. Kozuch, K. Ataka and J. Heberle: Surface-enhanced infrared absorption spectroscopy, Nat. Rev. Methods Primers **3** (2023) 70.

[19] P.J. Dobson: Nanoantenna Plasmon-Enhanced Spectroscopies for Biotechnological Applications, Contemp. Phys. **56** (2015) 506.

[20] B. Wiley, Y. Sun and Y. Xia: Polyol synthesis of silver nanostructures: control of product morphology with Fe (II) or Fe (III) species, Langmuir **21** (2005) 8077–8080.

[21] J. Ma and M. Zhan: Rapid production of silver nanowires based on high concentration of AgNO3 precursor and use of FeCl 3 as reaction promoter, RSC Adv. **4** (2014) 21060–21071.

[22] X. Tang and M. Tsuji: Syntheses of silver nanowires in liquid phase, Nanowires Science and Technology **402** (2010) 25–42.

[23] Q. Xue, W. Yao, J. Liu, Q. Tian, L. Liu, M. Li, Q. Lu, R. Peng and W. Wu: Facile synthesis of silver nanowires with different aspect ratios and used as high-performance flexible transparent electrodes, Nanoscale Res. Lett. **12** (2017) 480.

[24] A. Atanasova, T. Hristova-Vasileva and R. Todorov: Influence of the molecular weight and concentration of PVP on the polyol synthesized silver nanoparticles, J. Phys. Conf. Ser. **1762** (2021) 012032.

[25] K.T. Cao, K.K. Tran and H. Thi: Polyol method and surface functionalization of silver nanowires using bovine serum albumin for surface-enhanced Raman scattering application, Journal of Metals, Materials and Minerals **33** (2023) 1727.

[26] A.B.D. Nandiyanto, R. Oktiani and R. Ragadhita: How to read and interpret FTIR spectroscope of organic material, Indonesian Journal of Science and Technology **4** (2019) 97–118.

[27] J. Langer *et al.*: Present and future of surface-enhanced Raman scattering, ACS Nano **14** (2020) 28–117.

[28] H.-L. Wang, E.-M. You, R. Panneerselvam, S.-Y. Ding and Z.-Q. Tian: Advances of surface-enhanced Raman and IR spectroscopies: from nano/microstructures to macro-optical design, Light Sci. Appl. **10** (2021) 161.